HHS Public Access

Author manuscript

Biochemistry. Author manuscript; available in PMC 2021 December 21.

Published in final edited form as:

Biochemistry. 2018 January 23; 57(3): 324–333. doi:10.1021/acs.biochem.7b00974.

KRAS Switch Mutants D33E and A59G Crystallize in the State 1 Conformation

Jia Lu, **Asim K. Bera**, **Sudershan Gondi**, **Kenneth D. Westover***

Departments of Biochemistry and Radiation Oncology, The University of Texas Southwestern Medical Center at Dallas, Dallas, Texas 75390, United States

Abstract

KRAS switch loop movements play a crucial role in regulating RAS signaling, and alteration of these sensitive dynamics is a principal mechanism through which disease-associated RAS mutations lead to aberrant RAS activation. Prior studies suggest that despite a high degree of sequence similarity, the switches in KRAS are more dynamic than those in HRAS. We determined X-ray crystal structures of the rare tumorigenic KRAS mutants $KRAS^{D33E}$, in switch 1 (SW1), and $KRAS^{A59G}$, in switch 2 (SW2), bound to GDP and found these adopt nearly identical, open SW1 conformations as well as altered SW2 conformations. $KRAS^{A59G}$ bound to a GTP analogue crystallizes in the same conformation. This open conformation is consistent with the inactive "state 1" previously observed for HRAS bound to GTP. For $KRAS^{A59G}$, switch rearrangements may be regulated by increased flexibility in the ^{57}DXXGQ^{61} motif at codon 59. However, loss of interactions between side chains at codons 33 and 35 in the SW1 ^{33}DPT^{35} motif drives changes for $KRAS^{D33E}$. The ^{33}DPT^{35} motif is conserved for multiple members of the RAS subfamily but is not found in RAB, RHO, ARF, or Gα families, suggesting that dynamics mediated by this motif may be important for determining the selectivity of RAS–effector interactions. Biochemically, the consequence of altered switch dynamics is the same, showing impaired interaction with the guanine exchange factor SOS and loss of GAP-dependent GTPase activity. However, interactions with the RBD of RAF are preserved. Overall, these observations add to a body of evidence suggesting that HRAS and KRAS show meaningful differences in functionality stemming from differential protein dynamics independent of the hypervariable region.

Graphical Abstract

*Corresponding Author kenneth.westover@utsouthwestern.edu Phone: 214-645-7601.

Author Contributions

J.L. and A.K.B. contributed equally to this work.

Notes

The authors declare no competing financial interest.

ASSOCIATED CONTENT

Supporting Information

The Supporting Information is available free of charge on the ACSPublicationswebsite at DOI: 10.1021/acs.biochem.7b00974.

Nine supplementary figures (PDF)

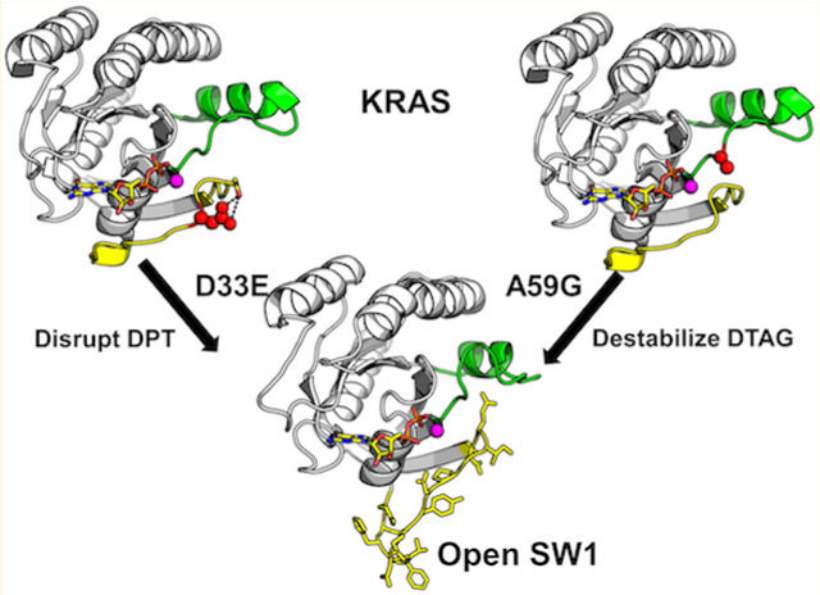

RAS proteins are positioned at the nexus of vital signaling pathways involved in cell growth, proliferation, differentiation, and survival and are often participatory, because of either oncogenic mutations or cellular addiction, in pathologic cellular states, particularly cancer.[1–3] Understanding the physiologic and pathologic functions of RAS requires building detailed models of RAS protein mechanics because ultimately the delicate conformational dynamics of RAS control key aspects of how RAS becomes activated and how signals are transmitted through RAS. Moreover, elucidating the effects that specific RAS mutations have on these dynamics will likely be required to discover effective direct approaches to addressing RAS-driven diseases in a tailored, allele-specific manner.[4,5]

RAS operates by cycling between active (GTP-bound) and inactive (GDP-bound) states. The primary structural changes between these occur in the switch domains, switch 1 (SW1, residues 25–40 in KRAS) and switch 2 (SW2, residues 60–76 in KRAS), which constitute a major portion of the guanine nucleotide binding pocket. The remainder of the protein is considerably less dynamic, although subtle changes can occur. In general, GDP-bound RAS has been observed with an open SW2 conformation, while GTP-bound RAS is more compact, with SW2 constrained by interactions with the γ-phosphate of GTP, a state termed state 2.[6,7] However, GTP-bound HRAS has also been observed in an open state called state 1, both for wild-type and mutant proteins, a form that has been proposed to represent an inactive transition state that may contribute to a dominant negative phenotype in some systems.[6,8–10] Co-crystal structures between RAS and RAS effectors have provided context for understanding the significance of switch movements. The structure of RAS and the guanine nucleotide exchange factor (GEF) SOS [Protein Data Bank (PDB) entry 1BKD][11,12] shows that GDP release, the rate-limiting step in exchange of GDP for GTP, is enabled by extending SW1 away from the main body of the protein, thereby breaking critical interactions between SW1 and GDP; the structure of RAS in complex with the GTPase-activating protein (GAP) P120GAP (PDB entry 1WQ1)[13] illustrates the required conformation of switch residues Gln25, Asp33, Ser39, Gln61, Glu62, Glu63, and Tyr64

to allow productive interactions with P120GAP that lead to catalysis of GTP hydrolysis. Likewise, crystal structures of RAS:RBD complexes (PDB entry 4G0N) illustrate critical interactions with Glu31, Asp33, Glu37, and Asp38 and the role of SW1 and SW2 dynamics in forming RAS–RAF interactions.[13,14] The importance of RAS switch dynamics in normal physiology is also underscored by demonstrations that SW2 dynamics can be a key differentiator of RAS subfamilies.[15] Moreover, recent biochemical and computational analyses have identified differences in RAS dynamics and function even for closely related RAS isoforms.[16,17]

We and others have hypothesized that disease-associated RAS mutations, most of which either occur in the switches themselves or cluster around the nucleotide binding site, function, in part, by altering switch dynamics, leading to RAS activation.[5,16,18] This view of how pathologic RAS may be activated complements well-established examples of certain mutations, such as KRAS G12D, that change the ability of RAS to cooperate with GAPs in GTP hydrolysis, thereby increasing the proportion of GTP-bound RAS in cells.[13] In addition to GAP insensitivity, the following hypotheses have been advanced as alternative mechanisms of RAS activation for particular RAS mutants. Activation may occur by (1) alterations in the strength of protein–protein interactions between RAS and its signaling effectors,[19] (2) GEF-independent RAS activation by enhancement of intrinsic nucleotide exchange rates as seen with KRAS G13D,[20–22] a common RAS mutation in colorectal cancer, or KRAS G12C, the most common RAS mutation in non-small cell lung cancer,[23,24] and (3) enhancement of GEF-dependent activation.[23,25]

SW1 and SW2 are physically adjacent, directly interact, and therefore influence the conformational states of one another. We hypothesized that operative principles regarding how these states are influenced or maintained could be ascertained by studying mutation-dependent changes in SW1 and SW2 dynamics and conducted structural studies of biologically active RAS mutations that occur in each of the switch domains. $KRAS^{D33E}$, a SW1 mutation, was identified as tumorigenic within a systematic genetic screen for identifying rare RAS gene variants and is constitutively activating for known RAS effector pathways.[26] Nevertheless, little else is known about its biochemical or structural properties. The $KRAS^{A59G}$ mutation, found in SW2, was also identified within the same screen as tumorigenic[26] and is similarly activating for RAS pathways. However, both mutations are infrequently observed in human populations.[27] The A59G mutation has also been studied in the context of HRAS to understand transition states for hydrolysis of GTP to GDP. Hall and colleagues determined an X-ray crystal structure of $HRAS^{A59G}$ showing conformational changes in SW2 and SW1.[18] Interestingly, Lukman and colleagues subsequently used molecular dynamics simulations to show that $HRAS^{A59G}$ and $KRAS^{A59G}$ fundamentally differ in their propensity to adopt an activated signaling state despite the fact that the sequences of these proteins are >90% identical outside of the hypervariable region.[16]

We determined crystal structures of these mutants and found that the GDP-bound forms show remarkably similar rearrangements of SW1 and SW2, with SW1 adopting a notably extended conformation consistent with state 1, previously identified in GTP-bound forms of $HRAS^{WT}$ and HRAS mutants.[6,8,9,28] GMPPCP-bound $KRAS^{A59G}$ also crystallizes in a similar form. Two sequence motifs appear to regulate these conformational changes. Finally,

we characterized the biochemical properties of these mutants, including GTP hydrolysis with GAP (p120), GDP dissociation with GEF (SOS), and relative binding affinity with RAF–RBD. The mutations showed GAP insensitivity but also a decreased number of GEF interactions. However, we also demonstrate that RAS–RBD interactions remain intact for the GTP-bound form, consistent with the fact that these mutants remain capable of activating MAPK pathways, leading to tumorigenesis.

MATERIALS AND METHODS

Protein Preparation and Crystallization.

Protein was expressed and purified as described previously.[29,30] Briefly, a construct encoding codon-optimized N-terminal His-tobacco etch virus (TEV)-D33E V-Ki-ras2 Kirsten rat sarcoma viral oncogene homologue (K-Ras) in the pJExpress vector (DNA2.0) was synthesized and used to transform BL21 (DE3) cells. Protein expression was induced with isopropyl β-D-1-thiogalactopyranoside and the soluble fraction of cell lysate subjected to Ni-NTA chromatography. The N-terminal His tag was cleaved by overnight digestion with TEV protease, and the TEV and tag were removed by reverse purification using Ni-NTA resin. The protein was further purified by Superdex75 in buffer [20 mM HEPES (pH 8.0), 150 mM NaCl, 5 mM $MgCl_2$, and 0.5 mM DTT]. $KRAS^{A59G}$ and $KRAS^{D33E}$ crystals grew by hanging drop vapor diffusion in 0.15 M cesium chloride, 15% PEG 3350, and 40 mM $MgCl_2$ and 0.1 M Tris (pH 8.5), 200 mM $MgCl_2$, and 25% PEG 3350, respectively. Protein purity is shown in Figure S1. Crystals were cryoprotected in mother liquor with 20% glycerol and flash-frozen in liquid nitrogen.

Crystal Structure Determination.

Diffraction images were collected at the Advanced Photon Source at beamline 19-ID (wavelength of 0.9795 Å). Data were integrated and scaled using HKL2000/3000 packages.[31] Molecular replacement was performed with KRAS WT (PDB entry 4OBE) as the search model using Phaser in Phenix software.[32,33] Manual and automated model building and refinement were performed using the Phenix package and Coot software.[32,33] Figures were prepared using Pymol (The PyMOL Molecular Graphics System, version 1.5.0.4, Schrödinger, LLC) and ChemDraw Professional version 15.0. Final model and scaled reflection data were deposited in the PDB (6ASA for $KRAS^{D33E}$-GDP, 6ASE for $KRAS^{A59G}$-GDP, and 6BP1 for $KRAS^{A59G}$-GMPPCP).

Nucleotide Exchange Assay.

KRAS protein (100 μM) was incubated with 300 μM Mant-GDP and 5 mM EDTA at room temperature for 2 h. Reactions were terminated with 10 mM $MgCl_2$, and then mixtures were buffer exchanged to remove EDTA and unbound nucleotides by using 2 mL of Zeba (ThermoFisher Scientific) desalting cartridges (7000 Da molecular weight cutoff) ino PBS with 2 mM $MgCl_2$. Proteins were adjusted to a final concentration of 2 μM and mixed with 4 μM GDP or 2 μM SOS with 4 μM GDP in a Corning 3820 384-well plate. Fluorescence was measured every 0.5 s for 5 min with excitation and emission set to 360 and 440 nm, respectively, in a Synergy Neo reader (BioTek). Data were exported and analyzed using GraphPad Prism (GraphPad Software, Inc.). All readings were performed in triplicate.

GTPase Assay.

KRAS proteins (2.5 mg/mL) in buffer [20 mmol/L Tris (pH 8.0) and 50 mM NaCl] were loaded with GTP at room temperature for 2 h by being exposed to exchange buffer containing EDTA. Proteins were buffer exchanged with assay buffer [30 mmol/L Tris (pH 7.5) and 1 mmol/L DTT], and the concentration was adjusted to 2 mg/mL. GTP loading was verified by back extraction of the nucleotide using 6 M urea and evaluation of nucleotide peaks by high-performance liquid chromatography using an ion exchange column as described previously.[15] The assay was performed in a clear 384-well plate (Costar) by combining GTP-loaded KRAS proteins (50 μM final concentration) with MESG (200 μM final concentration) and purine nucleotide phosphorylase (5 units/mL final concentration). GTP hydrol-ysis was initiated by the addition of $MgCl_2$ at a working concentration of 40 μM. For GAP stimulation, P120GAP was included at 50 μM. The absorbance at 360 nm was read every 8–15 s for 3600 s at 20 °C. All readings were performed in triplicate.

RAF Kinase Interaction Assay.

KRAS:RAF kinase interaction assays were performed as previously described.[34] Purified RAF kinase RBD was labeled with maleimide PEG biotin (Pierce) following the manufacturer's recommended protocol. Purified Flag-tagged KRAS (1 mg/mL) and KRAS mutants were loaded with GMPPNP (Sigma-Aldrich) by incubation for 2 h at 25 °C with a 50-fold excess of nucleotide in the presence of alkaline phosphatase (Thermo-Fisher). RAF–RBD–biotin was diluted to a final concentration of 40 nM and Flag-KRAS to 10 nM in assay buffer [20 mM Tris (pH 7.5), 100 mM NaCl, 1 mM $MgCl_2$, 5% glycerol, and 0.5% bovine serum albumin] and added to individual wells of a low-volume white 384-well plate (PerkinElmer). Complexes were disrupted by addition of a dilution series (from 2000 to 0.5 nM) of each mutant KRAS protein. The assay was developed by addition of a streptavidin donor and anti-Flag acceptor AlphaScreen beads (10 μg/mL). The α signal was measured after overnight incubation at 4 °C. All readings were performed in triplicate.

Molecular Dynamics (MD) Simulations.

The Schrödinger package on the Maestro platform (Schrödinger release 2016–2, Maestro, version 10.6, Schrödinger, LLC) was used to perform molecular dynamics. Systems were prepared from high-resolution crystal structures of Ras WT and mutants available in the PDB: H-Ras (4Q21 and 1LF0) and K-Ras (4OBE, 6ASA, and 6ASE). The Protein Preparation module was used for model construction, including adding missing atoms, H-bond assignments, and restrained minimization. All systems were neutralized by adding charge-neutralizing counterions with a 10 Å buffering distance in the SPC solvent model. No ion-excluded region was included. The 50 ns simulations were performed with the Desmond Molecular Dynamics module with a constant temperature (300 K) and pressure (1.0 bar) in the *NPT* ensemble.

RESULTS

Similar Conformations of Switches in KRAS^{D33E} and KRAS^{A59G}.

To understand the impact of specific KRAS mutations on a range of RAS functions, with the aim of discovering or informing new allele-specific RAS-directed therapeutic strategies, we have undertaken comprehensive structural and biochemical studies of disease-associated KRAS mutations.[19] As part of this work, we determined crystal structures of GDP-bound KRAS^{A59G} and KRAS^{D33E}. Both crystals were in orthorhombic space group $P2_12_12_1$ with similar unit cell dimensions. Crystallographic indices were excellent with reflections extending to 1.5 Å for KRAS^{A59G} and 2.5 Å for KRAS^{D33E}. Molecular replacement using KRAS WT (PDB entry 4OBE) as a search model was used to obtain phase information and the final model refined to an R_{work} of 18% and an R_{free} of 22% for KRAS^{A59G} and an R_{work} of 21% and an R_{free} of 26% for KRAS^{D33E} (Table 1). All expected regions of the protomers were visualized in the final electron densities, including SW1 and SW2.

SW1 and SW2 showed significant rearrangements in KRAS^{A59G} and KRAS^{D33E} compared to wild-type KRAS (PDB entry 4OBE), with SW1 notably extended away from the body of the protein (Figure 1A–C). The altered switch conformations were nearly identical between KRAS^{A59G} and KRAS^{D33E}, with His27, Phe28, and Val29 displaced from the nucleotide and the C_α atom of Phe28 shifted ~13 Å from its position in wild-type KRAS. Residues 24–26 are unwound from helix $\alpha 1$, and residues 30–36 are also shifted toward Phe28 as part of this remodeling. Therefore, the entire loop (from residue 25 to 38) is displaced from the nucleotide, leaving an exposed nucleotide binding pocket. However, the nucleotide ligand positions and magnesium ion binding sites are highly similar among KRAS WT, KRAS^{D33E}, and KRAS^{A59G} when structures are superimposed using the G domain. The extended SW1 conformation is supported primarily by the formation of hydrogen bonds of the backbone carbonyl of Val29 with the backbone nitrogen of His27, the amide side chain of Gln25 with the backbone nitrogen of Phe28, and the amide side chain of Asn26. SW2 is also altered with new interactions between the main chain N of Gln61 and the hydroxyl group of Tyr96 and weak electrostatic interactions between the side chain of Gln61 and His95. We note that within the crystal lattice SW1 and SW2 participate in contacts with adjacent molecules that have the potential to influence the switch conformations, although the A59G and D33E residues are not part of the interaction (Figure S2).

Our structures are highly similar to a conformation of HRAS previously observed in both solution and crystallographic studies called “state 1” (Figure 1D and Figure S3). State 1 was initially identified in HRAS T35S and T35A mutants as a conformation of GTP:HRAS that does not bind to RAF–RBD but can spontaneously convert to a closed state called state 2 that does bind.[8] A similar conformation has also been observed for HRAS^{WT},[9,28] HRAS^{G60A}, HRAS^{Y32F},[10,14,35] and MRAS^{WT}.[36] The fact that state 1 has been observed previously in multiple contexts suggests that this conformation is not a crystallographic artifact in our structures and may be biologically important. However, different than prior state 1 structures, our initial structures were obtained in the presence of GDP, as opposed to GTP or a GTP analogue.

Also, because HRAS^{A59G} has been structurally characterized to understand catalytic transition states, we compared the present KRAS structures to previously determined structures of HRAS^{A59G}.[16,18] Different from our structure, for GDP:HRAS^{A59G}, SW1 is not extended, and the conformations of HRAS WT and HRAS^{A59G} are highly similar (Figure 1E).[18] However, HRAS^{A59G} structures are notable for changes in SW2 with the α2 helix rotated toward the nucleotide relative to the WT structure such that SW2 occupies an intermediate position between GDP- and GTP-bound structures. SW2 conformations in our KRAS^{A59G} and KRAS^{D33E} structures are notable for moving closer to the p-loop relative to WT or HRAS structures, presumably because movement of SW1 creates additional space enabling interactions as described below (Figure 1F).

Mechanisms of Open Conformations of KRAS^{D33E} and KRAS^{A59G}.

The altered conformation of KRAS^{A59G} appears to be regulated by increased flexibility in the ^{57}DXXGQ^{61} motif of SW2 as a result of the KRAS^{A59G} mutation, consistent with previously reported molecular dynamics simulations,[37] allowing the main chain hydroxyl group to rotate toward SW2 and form a hydrogen bond with the side chain of Arg68. The reoriented Arg68 adopts a new conformation in which the second guanidinium nitrogen makes a hydrogen bond with the side chain of Glu37 (Figure 2A). Subsequently, the Ile36/Glu37/Asp38 peptide is pulled toward SW2 by these new interactions, and Tyr40 is also displaced toward SW2 by interacting with Asp38. This shift is further stabilized by interactions between the main chain carbonyl of Ile36 and Tyr40 through a water molecule. As a consequence, the side chain of Tyr32 is permitted space to interact with Asp38 and Tyr40, completing the hydrogen bond network within SW1 (Figure 2B). In both structures, the rearrangement at the distal end of SW1 is stabilized by a hydrogen bond network among residues Tyr32, Tyr40, and Asp38 via water molecules, although for the KRAS^{D33E} structure waters could not be discerned, possibly because of their dynamic nature. Although the final architectural rearrangement of the switches is similar between KRAS^{A59G} and KRAS^{D33E}, the mechanism for SW1 movement in the KRAS^{D33E} structure originates from a loss of interactions between the side chain of amino acid 33 and the highly conserved side chain of T35 as is observed in the WT structures of both KRAS:GDP (PDB entry 4OBE) and HRAS:GDP [PDB entry 4Q21 (Figure 2C)]. The conclusion that state 1 is promoted by loss of interactions between T35 and D33 is strengthened by the observation that mutations in T35 produce a highly similar conformation in HRAS.[8] Additionally, the KRAS^{D33E} structure features a slightly modified conformation of Arg68 that forms hydrogen bonds with the Gly60 and Glu63 main chain. When we compare our structures with HRAS^{WT} state 1 structures, the side chain of Arg68 in HRAS^{WT} adopts an intermediate position between what we observe in KRAS^{A59G} and KRAS^{D33E} but has interactions similar to those of KRAS^{A59G} with respect to the Arg68/Glu37/Ala59 network (Figure S4). These shifting interactions are consistent with the previously established role of Arg68 in regulating the state of switch 2.[18]

Molecular Dynamics of the DPT SW1 Motif.

Previously, molecular dynamics simulations suggested that the switches in KRAS are more dynamic than those in HRAS.[15,16] To further investigate these differences in the setting of the KRAS^{A59G} and KRAS^{D33E} switch mutations, we conducted molecular dynamics

simulations extending over 50 ns using structures of KRAS and HRAS as seed models. The following GDP-bound RAS structures were used as seed models for simulations: $KRAS^{WT}$ (4OBE), $KRAS^{A59G}$ (6ASE), $KRAS^{D33E}$ (6ASA), $HRAS^{WT}$ (4Q21), $HRAS^{A59G}$ (1LF5), and $HRAS^{D33Em}$ (manual mutation of Asp33 with Glu in $HRAS^{WT}$, PDB entry 4Q21). We used the protein RMSF (root-mean-square fluctuation) to compare the trajectories of each residue in each model over the time period of simulation. Comparison of $KRAS^{WT}$ and $HRAS^{WT}$ showed behavior consistent with previous MD simulations in which the SW2 conformation of KRAS is more dynamic than HRAS[16]-(Figure S5). Consistent with the altered switch conformations seen in the X-ray structures, comparison of $KRAS^{WT}$ with $KRAS^{A59G}$ (Figure 3A) and $KRAS^{D33E}$ (Figure 3B) showed an increase in the RMSF for switch regions. It should be noted that the same was true for HRAS simulations in which the D33E mutation was introduced computationally, but not for $HRAS^{A59G}$, consistent with crystal structures of $HRAS^{A59G}$ that do not show an extended SW1 conformation (Figure 3C,D). To further evaluate if increases in SW1 dynamics for $KRAS^{D33E}$ mutants correlate with losses of intramolecular hydrogen bonds in the DPT motif, we examined the distances between the side chain oxygen of T35 and the side chain oxygen of residue 33 (D or E) and the percentage of time a hydrogen bond is maintained between the side chains during simulations for HRAS and KRAS models (Figure 3E and Figure S6). These demonstrate a nearly total loss of intramolecular DPT H-bonds over the duration of the simulation in $KRAS^{A59G}$ and $KRAS^{D33E}$. On the other hand, H-bonds were seen between 35 and 62% of the simulation for $KRAS^{WT}$, $HRAS^{WT}$, and the HRAS mutants. Taken together, these results are consistent with the paradigm that the switch regions in KRAS are more dynamic at baseline, and this property is amplified when destabilizing mutations are introduced.

Biochemical Characterization of $KRAS^{D33E}$ and $KRAS^{A59G}$.

To understand the consequences of mutation-induced switch rearrangements on KRAS function, we characterized key biochemical properties of the KRAS mutants. KRAS has intrinsic GTPase activity that has been proposed to be important for autoinactivation, a process disrupted by certain RAS mutations such as codon 61 mutations that may contribute to their oncogenic activity.[19] Intrinsic GTPase activity is also important for some classes of direct RAS inhibitors that depend on the protein being GDP-bound.[38] In this reaction, RAS catalyzes GTP hydrolysis by neutralizing the negative charge at β- or γ-phosphate of GTP by a catalytic magnesium and residues Lys16, Tyr32, Thr35, and Gly60 and by correct positioning of a nucleophilic water that is stabilized by a conserved Gln at codon 61, in the SW2 conformation.[39] This activity is further stimulated by GAPs, such as P120GAP, which contribute an arginine residue that further delocalizes negative charge from the γ-phosphate.[40] Although our structures were determined with GDP-bound forms of RAS, they do show switch rearrangements, especially in the SW2 conformation, which could alter RAS enzymology. To determine the effect of $KRAS^{A59G}$ and $KRAS^{D33E}$ on intrinsic and GAP-stimulated GTPase activity for KRAS, we measure the rate of intrinsic GTP hydrolysis, as well as in response to P120GAP stimulation. We employed a purine nucleoside phosphorylase (PNP)-based assay to measure phosphate release in real time.[41] In our assay, the intrinsic rates are almost identical between the WT and mutants. On the other hand, GAP-stimulated GTP hydrolysis of two mutants markedly decreased activity relative to that of the WT (Figure 4A–C).

Because $KRAS^{A59G}$ and $KRAS^{D33E}$ present an open binding conformation and loss of several key interactions between the nucleotide and SW1, and because state 1 proteins have altered interactions with exchange factors, both positive[42] and negative,[10] we hypothesized that $KRAS^{A59G}$ may have altered nucleotide affinities or altered exchange rates. We used a previously reported method to measure nucleotide exchange kinetics by a fluorescently labeled GDP analogue (Mant-GDP).[19] This binding assay takes advantage of a shift in fluorescence emission from 441 to 432 nm when mant-GDP becomes unbound from RAS, allowing for monitoring of nucleotide dissociation in real time.[43] The kinetics of nucleotide exchange were statistically indistinguishable between mutants and the WT (Figure 4D,E). Given that state 1 structures have previously been implicated in biologically relevant interactions with SOS,[10] we also investigated if switch rearrangements could influence interactions between RAS and GEFs such as SOS, which interacts directly with both switches, although more extensively with SW1. In the presence of SOS, the two mutants exhibited no increase in the level of GDP dissociation when SOS was added, whereas WT showed substantial increases in GDP dissociation rates with the role of SOS in catalyzing GDP dissociation (Figure 4D,E and Table 2). This observation is similar to prior reports for the $HRAS^{G60A}$ state 1 mutant,[10] suggesting that the switch rearrangements seen for $KRAS^{A59G}$ and $KRAS^{D33E}$ result in lower levels of SOS-mediated nucleotide exchange relative to that of the WT.

Finally, we considered that rearrangements in SW1 could influence interactions between RAS and signaling effectors such as RAF. We therefore measured the relative binding affinity between KRAS and RAF using a sensitive AlphaScreen-based competition assay developed previously.[19] In this assay, we form complexes between labeled RAS and RAF, and then they compete with increasing concentrations of unlabeled RAS. Of note, all RAS proteins are preloaded with GMPPNP, a nonhydrolyzable GTP analogue. We observed no large differences in the binding of RAF to RAS mutants relative to that of the WT (Figure 4F and Table 2). This result contrasts with experiments performed with state 1, dominant negative mutant $HRAS^{G60A}$, where the mutant form showed a weakened ability to bind to RBD. However, these results are consistent with the fact that $KRAS^{D33E}$ and $KRAS^{A59G}$ can activate MAPK signaling in cellular systems.[26] In an attempt to capture $KRAS^{A59G}$ in state 2, as would be expected for RBD binding, we determined a crystal structure of $KRAS^{A59G}$ in complex with the GTP analogue GMPPCP at 2 Å. With the exception of the presence of clearly visible γ-phosphate, the structure was highly similar to the GDP-bound, state 1 structure (Figure S7). Considering the sum of biological, biochemical, and historical data about state 1 RAS structures, we conclude that $KRAS^{A59G}$ is capable of readily interconverting between states 1 and 2 as has been seen with HRAS structures.

DISCUSSION

Here we report crystal structures of $KRAS^{D33E}$ and $KRAS^{A59G}$ wherein SW1 assumes an almost identical extended conformation and similar, altered SW2 conformations that are consistent with state 1 observed for GTP-bound HRAS and MRAS. The structures are notably different from previously reported structures of GDP:$HRAS^{A59G}$ in which SW1 is closed. We further demonstrate the functional consequences of these rearrangements, including loss of interaction with SOS, but no change in intrinsic nucleotide dissociation

rates. These mutations also cause insensitivity to P120GAP-mediated stimulation of GTPase activity but do not preclude the ability of the activated protein to bind RBD, consistent with previously reported cellular data showing these mutations can result in accumulation of GTP:RAS that is competent to activate canonical RAS signaling pathways leading to tumor growth. In addition, we provide additional evidence that T35–D33 interaction regulates SW1 mechanics in RAS proteins that contain the DPT motif and further characterize the role of the ^{57}DXXGQ^{61} motif in SW2 for influencing SW1 dynamics.

Much of the early research on RAS structure and function was performed in the context of HRAS based on the assumption that the high degree of primary sequence identity and/or similarity between RAS isoforms would translate into similar biochemical and biological behaviors. Moreover, in many contexts, the biological functions of RAS isoforms appear to show redundancy.[44,45] Nevertheless, multiple recent studies have highlighted functional differences between RAS isoforms with a high degree of sequence identity or between disease-associated mutant forms of RAS.[5,19,46] Of particular interest are studies that begin to characterize the biophysical origins of these differences such as recent work showing origination from the allosteric G domain.[17] The current study adds to these findings by elaborating on the influence of RAS switch mutations on dynamics. At a minimum, these results provide evidence that HRAS and KRAS respond differently to the A59G mutation given differences in the GDP-bound structures. Additionally, these add support to the idea that KRAS is more dynamic in the switch regions than HRAS isoforms are based on the molecular dynamics and biochemical findings.

These results provide new insights into the role of the ^{57}DXXGQ^{61} motif in mediating SW1 flexibility. The conserved ^{57}DXXGQ^{61} motif is involved in Mg^{2+} coordination, GTP hydrolysis, and nucleotide exchange.[47,48] Interestingly, these studies demonstrate that HRAS and KRAS differ in how they respond to changes in the ^{57}DXXGQ^{61} motif. This is most immediately apparent in the difference between structures of HRAS^{A59G} and KRAS^{A59G}, where SW1 is closed in HRAS^{A59G} but open in KRAS^{A59G}. With respect to enzymology, it is worth noting that HRAS^{A59G} is generally considered to have an extremely slow GTP hydrolysis rate. In fact, this rate is slow enough that GTP-bound HRAS^{A59G} has been captured in a crystal structure, although in a complex with SOS.[12] However, in the study presented here, KRAS^{A59G} shows intrinsic GTP hydrolysis comparable to that of KRAS^{WT}. The apparent differences in GTP hydrolysis activities between KRAS and HRAS mutants might be rationalized as follows: while in the case of HRAS^{A59G}, extra flexibility introduced by Gly59 slows intrinsic GTPase activity presumably by allowing Gly60 to contact the γ-phosphate and stabilizing the GTP hydrolysis transition state,[18] in KRAS^{A59G} we see compensatory interactions between Gly59 and Arg68 that impose additional constraints that are favorable for hydrolysis. From an evolutionary perspective, it is interesting to note that within the RAS superfamily glycine substitutions equivalent to position 59 in KRAS are found in a handful of wild-type versions of other RAS proteins and, consistent with our structures, these RAS proteins also present open SW1 conformations (Figure S8).

We observed that the ^{33}DPT^{35} motif plays a critical role in regulating the dynamic behavior of switches for HRAS and KRAS. Our data showing that disruption of interactions between

D33 and T35 leads to increased flexibility in SW1 leading to state 1 are consistent with prior studies showing that T35A and T35S mutations in HRAS also result in state 1.[8] This feature may also hold significance for switch mechanics in other RAS superfamily members. Interestingly, when we examine the sequence conservation of this motif within the RAS superfamily, we note that although ^{33}DPT^{35} appears in a large segment of the RAS subfamily, in other subfamilies it is absent, being replaced by an NPT (N for nonpolar residues) (RHO and ARF families) or XXT motif (RAB family) (Figure S9). For NPT and XXT motifs, no molecular interactions between structurally equivalent positions 33 and 35 are predicted to occur. However, for KRAS and HRAS, DPT forms an intramolecular interaction that appears to contribute a degree of regulation for SW1 dynamics. This structural feature could be important for achieving selectivity in interactions with GEFs or other RAS effectors that have extensive contacts with SW1.

These data also highlight the conformational dependency of SW1 and SW2 upon one another. While we were not surprised that a mutation in SW1 could perturb its conformation, it was surprising that a SW2 conformation could produce the effect we saw in SW1. Nevertheless, this observation is recapitulated by prior studies, such as those on HRAS^{A60G}, arguing for its biological significance. Moreover, we noticed in MD simulations that introduction of the KRAS^{D33E} mutation increased the flexibility of SW1 and also increased the flexibility of SW2 (Figure 3C). Our crystal structures also showed a poorly constrained, open SW1 while at the same time altering SW2 through interactions with loop 4 that draw it closer to the binding site. This may contribute to the decreased level of SOS-dependent exchange of GDP for GTP we and others have observed.[10] When taken in the context of prior data, our data suggest that ^{33}DPT^{35} and ^{57}DXXGQ^{61} may gate conformational communication between SW1 and SW2 in both GDP and GTP states. Overall, these results demonstrate how movements in SW1 lead to subtle but possibly important changes in the conformation of SW2 that have an impact on RAS function related to nucleotide hydrolysis or RAS–effector interactions.

A better understanding of RAS switch mechanics may have implications for the next generation of therapeutic strategies aimed directly at RAS. The discovery of a new class of covalent inhibitors of KRAS^{G12C}, the most common RAS mutation in lung cancer, has raised the possibility of developing new clinical therapies that function in an ultratargeted fashion, depending on the very mutation that activates KRAS, for efficacy.[24,29,30,38,49] These compounds were serendipitously discovered to bind to a pocket adjacent to SW2 that forms only with movement of SW2. Subsequent studies have detailed how certain features of this class of inhibitors can further influence switch dynamics.[50–52] Although highly speculative, the extended conformation of SW1 we see in this study could have implications for development of new classes of SW2 compounds that also access pockets made by SW1 movements or development of compounds that target SW1 pockets exclusively.

In summary, we have determined X-ray structures of tumorigenic KRAS^{A59G} and KRAS^{D33E} mutants in the GDP-bound form and KRAS^{A59G} GTP-bound form with a notably extended conformation of SW1 and alteration of SW2 consistent with previously documented GTP:HRAS state 1 structures. While some biochemical properties, such as impaired GAP-stimulated GTP hydrolysis, can be rationalized on the basis of these

structures, other properties such as maintenance of RBD binding are not, arguing that these KRAS mutants must rapidly interconvert between states 1 and 2. These results may help explain non-intuitive differences between the highly similar KRAS and HRAS proteins and improve our understanding of functional distinctions between certain branches of the RAS superfamily. Finally, these findings may have implications for new direct approaches to therapeutic targeting of RAS.

Supplementary Material

Refer to Web version on PubMed Central for supplementary material.

ACKNOWLEDGMENTS

The authors thank the staff at the structural biology laboratory at the University of Texas Southwestern Medical Center and at beamline 19ID of the Advanced Photon Source for discussions and technical assistance with X-ray data collection and processing. Results shown in this report were derived from work performed at Argonne National Laboratory, Structural Biology Center, at the Advanced Photon Source. Argonne is operated by the University of Chicago Argonne, LLC, for the U.S. Department of Energy, Office of Biological and Environmental Research, under Contract DE-AC02–06CH11357.

Funding

National Institutes of Health Grant U54 CA196519 (K.D.W.), U.S. Department of Defense Grant W81XWH-16–1-0106 (K.D.W.), and Jimmy V Foundation (K.D.W.).

REFERENCES

(1). Prior IA, Lewis PD, and Mattos C. (2012) A comprehensive survey of Ras mutations in cancer,. Cancer Res. 72, 2457–2467. [PubMed: 22589270]

(2). Stephen AG, Esposito D, Bagni RK, and McCormick F. (2014) Dragging ras back in the ring. Cancer Cell 25, 272–281. [PubMed: 24651010]

(3). Pylayeva-Gupta Y, Grabocka E, and Bar-Sagi D. (2011) RAS oncogenes: weaving a tumorigenic web. Nat. Rev. Cancer 11, 761. [PubMed: 21993244]

(4). Montalvo SK, Li L, and Westover KD (2017) Rationale for RAS mutation-tailored therapies. Future Oncol. 13, 263–271. [PubMed: 27728979]

(5). Haigis KM (2017) KRAS Alleles: The Devil Is in the Detail. Trends in Cancer 3, 686. [PubMed: 28958387]

(6). Spoerner M, Hozsa C, Poetzl JA, Reiss K, Ganser P, Geyer M, and Kalbitzer HR (2010) Conformational states of human rat sarcoma (Ras) protein complexed with its natural ligand GTP and their role for effector interaction and GTP hydrolysis. J. Biol. Chem. 285, 39768–39778. [PubMed: 20937837]

(7). Kalbitzer H, and Spoerner M. (2013) State 1 (T) inhibitors of activated Ras. Enzymes 33, 69–94. [PubMed: 25033801]

(8). Spoerner M, Herrmann C, Vetter IR, Kalbitzer HR, and Wittinghofer A. (2001) Dynamic properties of the Ras switch I region and its importance for binding to effectors. Proc. Natl. Acad. Sci. U. S. A. 98, 4944–4949. [PubMed: 11320243]

(9). Araki M, Shima F, Yoshikawa Y, Muraoka S, Ijiri Y, Nagahara Y, Shirono T, Kataoka T, and Tamura A. (2011) Solution structure of the state 1 conformer of GTP-bound H-Ras protein and distinct dynamic properties between the state 1 and state 2 conformers. J. Biol. Chem. 286, 39644–39653. [PubMed: 21930707]

(10). Ford B, Skowronek K, Boykevisch S, Bar-Sagi D, and Nassar N. (2005) Structure of the G60A Mutant of Ras IMPLICATIONS FOR THE DOMINANT NEGATIVE EFFECT. J. Biol. Chem. 280, 25697–25705. [PubMed: 15878843]

(11). Boriack-Sjodin PA, Margarit SM, Bar-Sagi D, and Kuriyan J. (1998) The structural basis of the activation of Ras by Sos,. Nature 394, 337. [PubMed: 9690470]

(12). Margarit SM, Sondermann H, Hall BE, Nagar B, Hoelz A, Pirruccello M, Bar-Sagi D, and Kuriyan J. (2003) Structural evidence for feedback activation by Ras· GTP of the Ras-specific nucleotide exchange factor SOS. Cell 112, 685–695. [PubMed: 12628188]

(13). Scheffzek K, Ahmadian MR, Kabsch W, Wiesmüller L, Lautwein A, Schmitz F, and Wittinghofer A. (1997) The Ras-RasGAP complex: structural basis for GTPase activation and its loss in oncogenic Ras mutants,. Science 277, 333–339. [PubMed: 9219684]

(14). Fetics SK, Guterres H, Kearney BM, Buhrman G, Ma B, Nussinov R, and Mattos C. (2015) Allosteric effects of the oncogenic RasQ61L mutant on Raf-RBD. Structure 23, 505–516. [PubMed: 25684575]

(15). Harrison RA, Lu J, Carrasco M, Hunter J, Manandhar A, Gondi S, Westover KD, and Engen JR (2016) Structural Dynamics in Ras and Related Proteins upon Nucleotide Switching. J. Mol. Biol. 428, 4723–4735. [PubMed: 27751724]

(16). Lukman S, Grant BJ, Gorfe AA, Grant GH, and McCammon JA (2010) The distinct conformational dynamics of K-Ras and H-Ras A59G. PLoS Comput. Biol. 6, e1000922. [PubMed: 20838576]

(17). Johnson CW, Reid D, Parker JA, Salter S, Knihtila R, Kuzmic P, and Mattos C. (2017) The small GTPases K-Ras, N-Ras, and H-Ras have distinct biochemical properties determined by allosteric effects,. J. Biol. Chem. 292, 12981–12993. [PubMed: 28630043]

(18). Hall BE, Bar-Sagi D, and Nassar N. (2002) The structural basis for the transition from Ras-GTP to Ras-GDP,. Proc. Natl. Acad. Sci. U. S. A. 99, 12138–12142. [PubMed: 12213964]

(19). Hunter JC, Manandhar A, Carrasco MA, Gurbani D, Gondi S, and Westover KD (2015) Biochemical and structural analysis of common cancer-associated KRAS mutations. Mol. Cancer Res. 13, 1325–1335. [PubMed: 26037647]

(20). Lu J, Hunter J, Manandhar A, Gurbani D, and Westover KD (2015) Structural dataset for the fast-exchanging KRAS G13D. Data in Brief 5, 572–578. [PubMed: 26958611]

(21). Palmioli A, Sacco E, Airoldi C, Di Nicolantonio F, D'Urzo A, Shirasawa S, Sasazuki T, Di Domizio A, De Gioia L, Martegani E, Bardelli A, Peri F, and Vanoni M. (2009) Selective cytotoxicity of a bicyclic Ras inhibitor in cancer cells expressing K-RasG13D. Biochem. Biophys. Res. Commun. 386, 593–597. [PubMed: 19540195]

(22). Smith MJ, Neel BG, and Ikura M. (2013) NMR-based functional profiling of RASopathies and oncogenic RAS mutations. Proc. Natl. Acad. Sci. U. S. A. 110, 4574–4579. [PubMed: 23487764]

(23). Lito P, Solomon M, Li LS, Hansen R, and Rosen N. (2016) Allele-specific inhibitors inactivate mutant KRAS G12C by a trapping mechanism. Science 351, 604–608. [PubMed: 26841430]

(24). Patricelli MP, Janes MR, Li L-S, Hansen R, Peters U, Kessler LV, Chen Y, Kucharski JM, Feng J, Ely T, Chen JH, Firdaus SJ, Babbar A, Ren P, and Liu Y. (2016) Selective inhibition of oncogenic KRAS output with small molecules targeting the inactive state. Cancer Discovery 6, 316–329. [PubMed: 26739882]

(25). Vigil D, Cherfils J, Rossman KL, and Der CJ (2010) Ras superfamily GEFs and GAPs: validated and tractable targets for cancer therapy? Nat. Rev. Cancer 10, 842. [PubMed: 21102635]

(26). Kim E, Ilic N, Shrestha Y, Zou L, Kamburov A, Zhu C, Yang X, Lubonja R, Tran N, Nguyen C, Lawrence MS, Piccioni F, Bagul M, Doench JG, Chouinard CR, Wu X, Hogstrom L, Natoli T, Tamayo P, Horn H, Corsello SM, Lage K, Root DE, Subramanian A, Golub TR, Getz G, Boehm JS, and Hahn WC (2016) Systematic Functional Interrogation of Rare Cancer Variants Identifies Oncogenic Alleles. Cancer Discovery 6, 714–726. [PubMed: 27147599]

(27). Bamford S, Dawson E, Forbes S, Clements J, Pettett R, Dogan A, Flanagan A, Teague J, Futreal PA, Stratton MR, and Wooster R. (2004) The COSMIC (Catalogue of Somatic Mutations in Cancer) database and website,. Br. J. Cancer 91, 355. [PubMed: 15188009]

(28). Muraoka S, Shima F, Araki M, Inoue T, Yoshimoto A, Ijiri Y, Seki N, Tamura A, Kumasaka T, Yamamoto M, and Kataoka T. (2012) Crystal structures of the state 1 conformations of the GTP-bound H-Ras protein and its oncogenic G12V and Q61L mutants. FEBS Lett. 586, 1715–1718. [PubMed: 22584058]

(29). Lim SM, Westover KD, Ficarro SB, Harrison RA, Choi HG, Pacold ME, Carrasco M, Hunter J, Kim ND, Xie T, Sim T, Janne PA, Meyerson M, Marto JA, Engen JR, and Gray NS (2014) Therapeutic targeting of oncogenic K-Ras by a covalent catalytic site inhibitor. Angew. Chem., Int. Ed. 53, 199–204.

(30). Hunter JC, Gurbani D, Ficarro SB, Carrasco MA, Lim SM, Choi HG, Xie T, Marto JA, Chen Z, Gray NS, and Westover KD (2014) In situ selectivity profiling and crystal structure of SML-8–73–1, an active site inhibitor of oncogenic K-Ras G12C. Proc. Natl. Acad. Sci. U. S. A. 111, 8895–8900. [PubMed: 24889603]

(31). Otwinowski Z, and Minor W. (1997) Processing of X-ray diffraction data collected in oscillation mode. Methods Enzymol. 276, 307–326.

(32). Adams PD, Afonine PV, Bunkoczi G, Chen VB, Davis IW, Echols N, Headd JJ, Hung LW, Kapral GJ, Grosse-Kunstleve RW, McCoy AJ, Moriarty NW, Oeffner R, Read RJ, Richardson DC, Richardson JS, Terwilliger TC, and Zwart PH (2010) PHENIX: a comprehensive Python-based system for macromolecular structure solution. Acta Crystallogr., Sect. D: Biol. Crystallogr. 66, 213–221. [PubMed: 20124702]

(33). Emsley P, Lohkamp B, Scott WG, and Cowtan K. (2010) Features and development of Coot. Acta Crystallogr., Sect. D: Biol. Crystallogr. 66, 486–501. [PubMed: 20383002]

(34). Lim SM, Westover KD, Ficarro SB, Harrison RA, Choi HG, Pacold ME, Carrasco M, Hunter J, Kim ND, Xie T, Sim T, Janne PA, Meyerson M, Marto JA, Engen JR, and Gray NS (2014) Therapeutic Targeting of Oncogenic K-Ras by a Covalent Catalytic Site Inhibitor. Angew. Chem., Int. Ed. 53, 199–204.

(35). Shima F, Ijiri Y, Muraoka S, Liao J, Ye M, Araki M, Matsumoto K, Yamamoto N, Sugimoto T, Yoshikawa Y, Kumasaka T, Yamamoto M, Tamura A, and Kataoka T. (2010) Structural basis for conformational dynamics of GTP-bound Ras protein. J. Biol. Chem. 285, 22696–22705. [PubMed: 20479006]

(36). Ye M, Shima F, Muraoka S, Liao J, Okamoto H, Yamamoto M, Tamura A, Yagi N, Ueki T, and Kataoka T. (2005) Crystal structure of M-Ras reveals a GTP-bound “off” state conformation of Ras family small GTPases. J. Biol. Chem. 280, 31267–31275. [PubMed: 15994326]

(37). Scott KA, Alonso DO, Sato S, Fersht AR, and Daggett V. (2007) Conformational entropy of alanine versus glycine in protein denatured states. Proc. Natl. Acad. Sci. U. S. A. 104, 2661–2666. [PubMed: 17307875]

(38). Ostrem JM, Peters U, Sos ML, Wells JA, and Shokat KM (2013) K-Ras (G12C) inhibitors allosterically control GTP affinity and effector interactions. Nature 503, 548–551. [PubMed: 24256730]

(39). Li G, and Zhang XC (2004) GTP hydrolysis mechanism of Ras-like GTPases. J. Mol. Biol. 340, 921–932. [PubMed: 15236956]

(40). Ahmadian MR, Stege P, Scheffzek K, and Wittinghofer A. (1997) Confirmation of the arginine-finger hypothesis for the GAP-stimulated GTP-hydrolysis reaction of Ras. Nat. Struct. Biol. 4, 686–689. [PubMed: 9302992]

(41). Nixon AE, Hunter JL, Bonifacio G, Eccleston JF, and Webb MR (1998) Purine nucleoside phosphorylase: its use in a spectroscopic assay for inorganic phosphate and for removing inorganic phosphate with the aid of phosphodeoxyribomutase. Anal. Biochem. 265, 299–307. [PubMed: 9882406]

(42). Kalbitzer HR, Spoerner M, Ganser P, Hozsa C, and Kremer W. (2009) Fundamental link between folding states and functional states of proteins. J. Am. Chem. Soc. 131, 16714–16719. [PubMed: 19856908]

(43). Eccleston J, Moore K, Brownbridge G, Webb M, and Lowe P. (1991) Fluorescence approaches to the study of the p21ras GTPase mechanism. Biochem. Soc. Trans. 19, 432. [PubMed: 1889625]

(44). Drosten M, Dhawahir A, Sum EY, Urosevic J, Lechuga CG, Esteban LM, Castellano E, Guerra C, Santos E, and Barbacid M. (2010) Genetic analysis of Ras signalling pathways in cell proliferation, migration and survival. EMBO J. 29, 1091–1104. [PubMed: 20150892]

(45). Castellano E, and Santos E. (2011) Functional specificity of ras isoforms: so similar but so different. Genes Cancer 2, 216–231. [PubMed: 21779495]

(46). Kapoor A, and Travesset A. (2015) Differential dynamics of RAS isoforms in GDP-and GTP-bound states, Proteins: Structure. Proteins: Struct., Funct., Genet. 83, 1091–1106. [PubMed: 25846136]

(47). Sung YJ, Hwang MC, and Hwang YW (1996) The dominant negative effects of H-Ras harboring a Gly to Ala mutation at position 60,. J. Biol. Chem. 271, 30537–30543. [PubMed: 8940023]

(48). Mistou MY, Jacquet E, Poullet P, Rensland H, Gideon P, Schlichting I, Wittinghofer A, and Parmeggiani A. (1992) Mutations of Ha-ras p21 that define important regions for the molecular mechanism of the SDC25 C-domain, a guanine nucleotide dissociation stimulator. EMBO J. 11, 2391–2397. [PubMed: 1628612]

(49). Xiong Y, Lu J, Hunter J, Li L, Scott D, Choi HG, Lim SM, Manandhar A, Gondi S, Sim T, Westover KD, and Gray NS (2017) Covalent Guanosine Mimetic Inhibitors of G12C KRAS. ACS Med. Chem. Lett. 8, 61–66. [PubMed: 28105276]

(50). Lu J, Harrison RA, Li L, Zeng M, Gondi S, Scott D, Gray NS, Engen JR, and Westover KD (2017) KRAS G12C Drug Development: Discrimination between Switch II Pocket Configurations Using Hydrogen/Deuterium-Exchange Mass Spectrometry. Structure 25, 1442. [PubMed: 28781083]

(51). Zeng M, Lu J, Li L, Feru F, Quan C, Gero TW, Ficarro SB, Xiong Y, Ambrogio C, Paranal RM, Catalano M, Shao J, Wong KK, Marto JA, Fischer ES, Janne PA, Scott DA, Westover KD, and Gray NS (2017) Potent and Selective Covalent Quinazoline Inhibitors of KRAS G12C. Cell Chem. Biol. 24, 1005. [PubMed: 28781124]

(52). McGregor LM, Jenkins ML, Kerwin C, Burke JE, and Shokat KM (2017) Expanding the Scope of Electrophiles Capable of Targeting K-Ras Oncogenes. Biochemistry 56, 3178. [PubMed: 28621541]

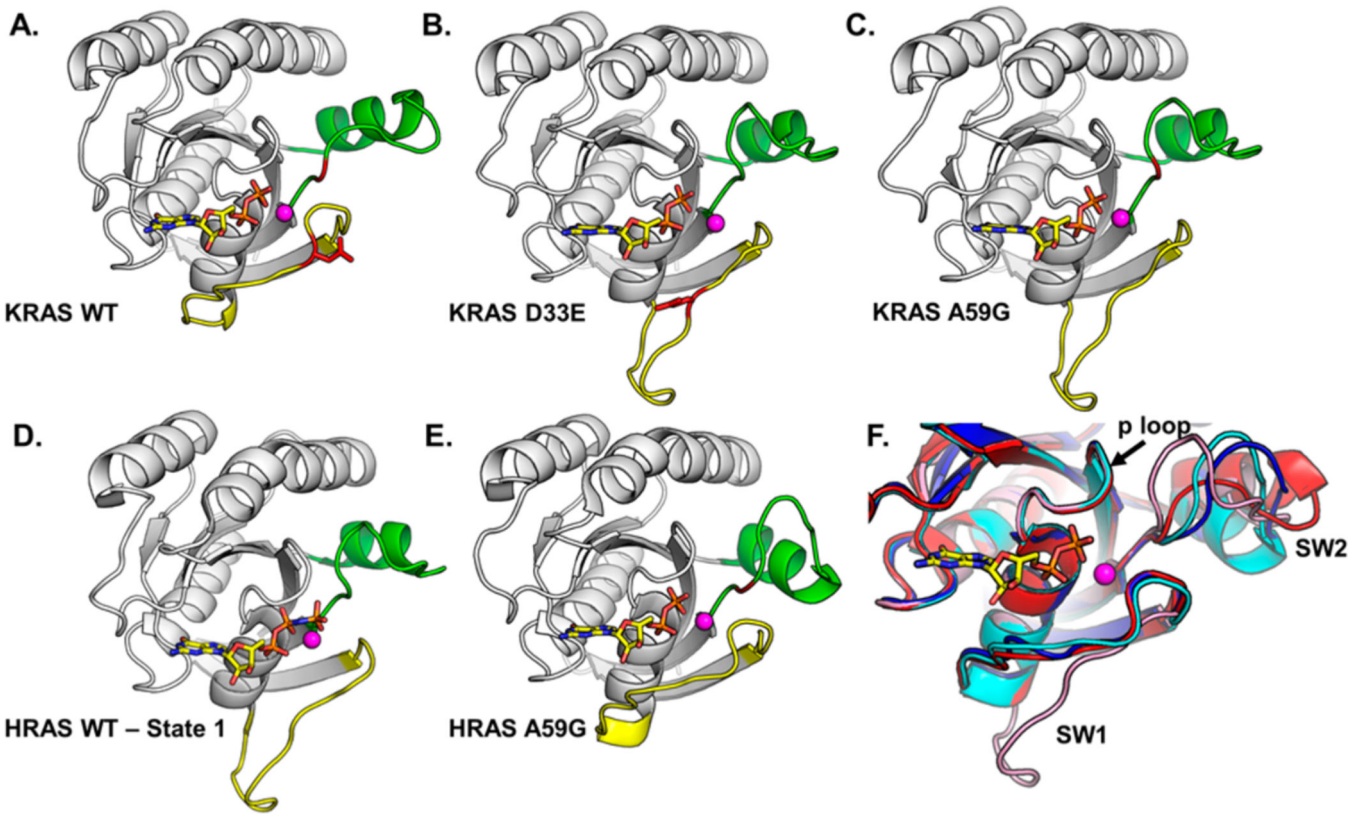

Figure 1.

Comparison of RAS structures. (A) $KRAS^{WT}$ (4OBE), codons 33 and 59 colored red. (B) $KRAS^{D33E}$, residue 33 colored red. (C) $KRAS^{A59G}$, residue 59 colored red. (D) HRAS WT (4EFL). (E) $HRAS^{A59G}$-GDP (1LF5), A59G colored red. In panels A–D, SW1 is colored yellow, SW2 green, and Mg^{2+} magenta. (F) Superposition of $KRAS^{WT}$ (red), $KRAS^{A59G}$ (pink), $HRAS^{WT}$ (4Q21, blue), and $HRAS^{A59G}$ (cyan).

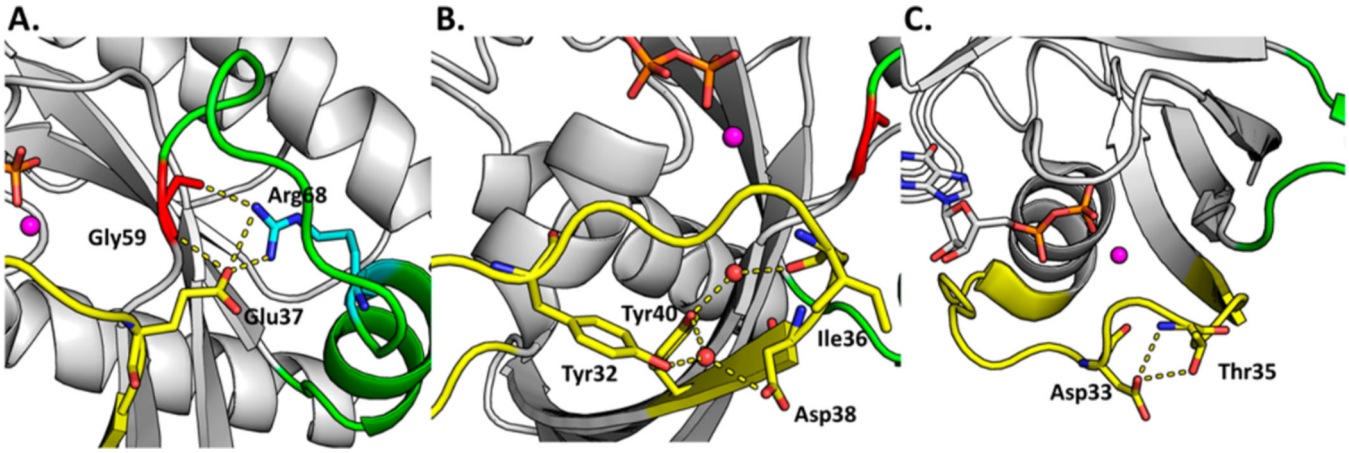

Figure 2.

Mechanisms of SW1 rearrangements. (A) KRAS A59G increases flexibility in the backbone leading to new interactions with Glu37 and Arg68. (B) Interactions among Tyr32, Ile36, Asp38, Tyr40, and waters support an extended SW1 conformation in KRAS A59G. (C) The DPT SW1 motif in HRAS WT structures (PDB entry 4Q21) is characterized by interactions between Asp33 and Thr35. For all panels, SW1 is colored yellow and SW2 green.

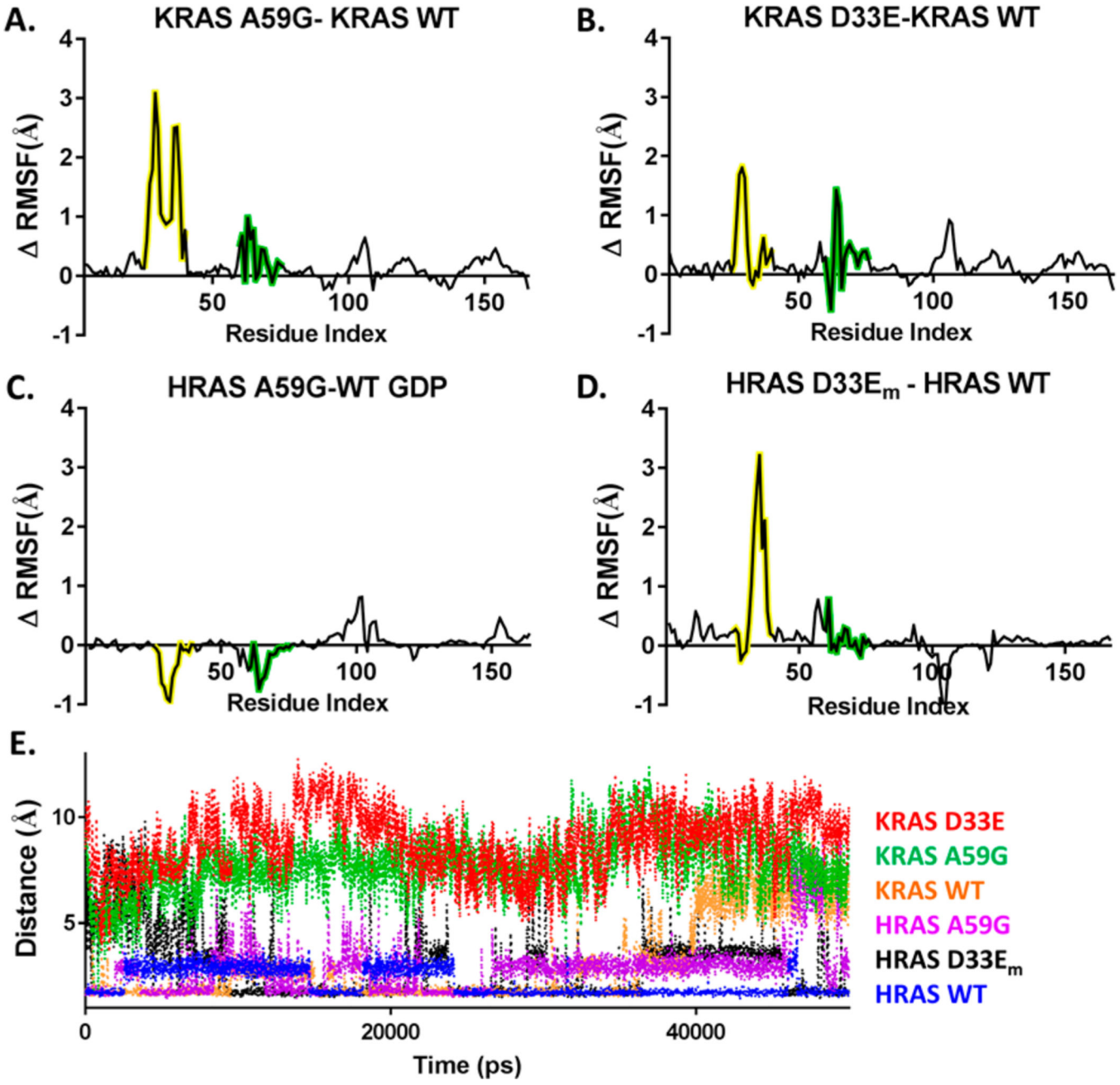

Figure 3.

MD simulations of RAS proteins. The RMSF is used to characterize translations of the protein backbone residues during the MD time course. Differences in RMSF (ΔRMSF, in angstroms) are calculated to indicate the difference between (A) $KRAS^{A59G}$ and WT, (B) $KRAS^{D33E}$ and WT, (C) $HRAS^{A59G}$ and WT, and (D) $HRAS^{D33Em}$ and WT. (E) KRAS simulations show increased dynamics in SW1. Distances between side chains of residues 33 and 35 are plotted over time for all structures.

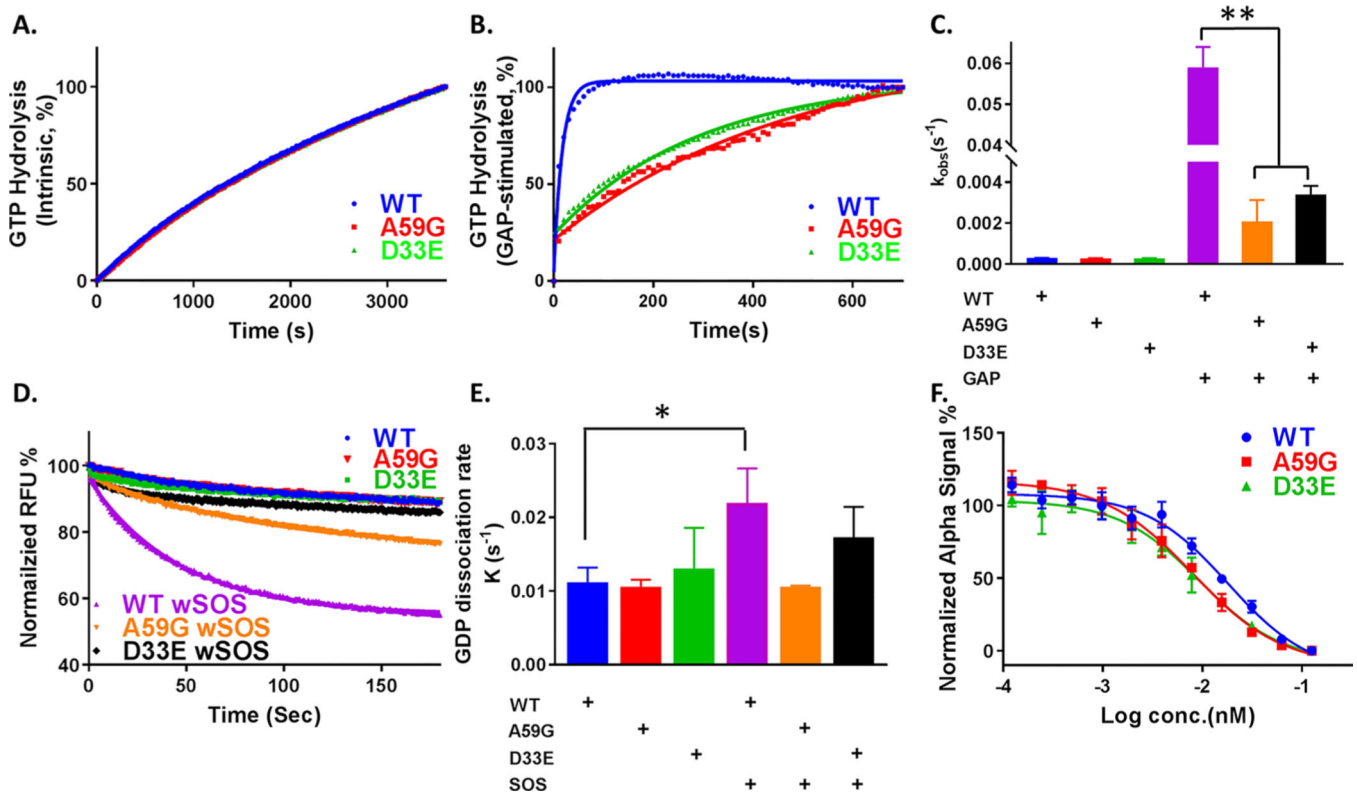

Figure 4.

Biochemical analysis of KRAS WT (blue), A59G (red), and D33E (green). (A) Intrinsic GTP hydrolysis and (B) GAP-stimulated GTP hydrolysis were assessed by continuously measuring phosphate using a PNP-based colorimetric assay. (C) First-order rates of both intrinsic and GAP-stimulated GTP hydrolysis. (D) RAS:GDP dissociation-dependent changes in fluorescence using mant-GDP. Experiments were performed with or without SOS. (E) First-order rates calculated from panel D. (F) Relative affinity of WT and mutants for RAF-RBD.

Table 1.

Data Collection and Refinement Statistics

	6ASA (KRAS^{D33E}-GDP)	6ASE (KRAS^{A59G}-GDP)	6BP1 (KRAS^{A59G}-GCP)
	Data Collection		
space group	$P2_12_12_1$	$P2_12_12_1$	$P2_12_12_1$
cell parameters			
a, *b*, *c* (Å)	34.53, 47.08, 90.77	34.43, 47.43, 89.70	34.39, 47.47, 89.66
α, β, γ (deg)	90.00, 90.00, 90.00	90.00, 90.00, 90.00	90.00, 90.00, 90.00
resolution (highest shell) (Å)	50.00–2.54 (2.59–2.54)	32.59–1.55 (1.58–1.55)	50–2.00 (2.03–2.00)
no. of unique reflections	4713	21220	10450
redundancy	4.1 (2.8)	6.7 (2.9)	5.8 (5.8)
completeness (last shell) (%)	90.3 (60.4)	97.2 (78.2)	99.9 (100.0)
I/σ(I) (last shell)	15.8 (1.8)	23.76 (1.23)	20.32 (5.37)
R_{merge} (last shell)[a]	0.080 (0.356)	0.088 (0.815)	0.093 (0.315)
	Refinement		
resolution range (Å)	32.67–2.54	32.59–1.55	32.55–2.01
no. of reflections used	4695	21220	10405
no. of protein atoms	1342	1376	1355
no. of water molecules	2	111	92
no. of metal ions	1	1	0
no. of ligand atoms	28	28	33
R_{work} [b]	0.21	0.17	0.20
R_{free} [c]	0.26	0.21	0.22
root-mean-square deviation			
bond lengths (Å)	0.002	0.007	0.002
bond angles (deg)	0.489	1.082	0.421
Ramachandran plot (%)			
favored	97.0	98.0	98.2
allowed	3.0	2.0	1.8
outliers	0.0	0.0	0.0

	6ASA (KRAS^{D33E}-GDP)	6ASE (KRAS^{A59G}-GDP)	6BP1 (KRAS^{A59G}-GCP)
average B-factor (Å^2)			
protein	55.6	32.0	34.6
ligand	53.5	28.1	38.8
metal	47.4	24.9	
water	35.0	37.1	35.0

[a] $R_{merge} = \sum|I - (I)|/\sum I$, where I is the intensity of an observed reflection and (I) is the average intensity of multiple observations.

[b] $R_{work} = \sum||F_{obs}| - |F_{cal}||/\sum|F_{obs}|$.

[c] $R_{free} = \sum||F_{obs}| - |F_{cal}||/\sum|F_{obs}|$, where F_{obs} is from a test set of reflections that are not used in structural refinement.

Table 2.

Results of Biochemical Assays

	GDP dissociation *k* ($\times 10^{-3}$ s^{-1})	**GTP hydrolysis *k* ($\times 10^{-4}$ s^{-1})**	**relative RAF kinase affinity (nM)**
WT	11.2 ± 2.0	2.9 ± 0.3	19.4 ± 7.2
A59G	10.6 ± 1.0	2.8 ± 0.5	8.4 ± 1.7
D33E	13.1 ± 5.5	2.8 ± 0.4	9.8 ± 1.8
WT and SOS	22.0 ± 4.7	-	-
A59G and SOS	10.6 ± 0.2	-	-
D33E and SOS	17.3 ± 4.1	-	-
WT and p120	-	590 ± 50.3	-
A59G and p120	-	20.5 ± 5.2	-
D33E and p120	-	34.2 ± 1.9	-